



Article

# Rapid Characterization of Formulated Pharmaceuticals Using Fast MAS 1H Solid-State NMR Spectroscopy

David A. Hirsh, Anuradha Viraj Wijesekara, Scott L. Carnahan, Ivan Hung, Joseph W. Lubach, Karthik Nagapudi, and Aaron James Rossini

Mol. Pharmaceutics, Just Accepted Manuscript • Publication Date (Web): 16 May 2019

Downloaded from http://pubs.acs.org on May 16, 2019

#### **Just Accepted**

"Just Accepted" manuscripts have been peer-reviewed and accepted for publication. They are posted online prior to technical editing, formatting for publication and author proofing. The American Chemical Society provides "Just Accepted" as a service to the research community to expedite the dissemination of scientific material as soon as possible after acceptance. "Just Accepted" manuscripts appear in full in PDF format accompanied by an HTML abstract. "Just Accepted" manuscripts have been fully peer reviewed, but should not be considered the official version of record. They are citable by the Digital Object Identifier (DOI®). "Just Accepted" is an optional service offered to authors. Therefore, the "Just Accepted" Web site may not include all articles that will be published in the journal. After a manuscript is technically edited and formatted, it will be removed from the "Just Accepted" Web site and published as an ASAP article. Note that technical editing may introduce minor changes to the manuscript text and/or graphics which could affect content, and all legal disclaimers and ethical guidelines that apply to the journal pertain. ACS cannot be held responsible for errors or consequences arising from the use of information contained in these "Just Accepted" manuscripts.



# Rapid Characterization of Formulated

# Pharmaceuticals Using Fast MAS <sup>1</sup>H Solid-State

# NMR Spectroscopy

David A. Hirsh, <sup>1#</sup> Anuradha V. Wijesekara, <sup>1#</sup> Scott L. Carnahan, <sup>1</sup> Ivan Hung, <sup>2</sup> Joseph W.

Lubach, <sup>3\*</sup> Karthik Nagapudi, <sup>3\*</sup> and Aaron J. Rossini <sup>I\*</sup>

### **AUTHOR INFORMATION**

#DAH and AVW contributed equally to this work.

## **Corresponding Authors**

\*e-mail: arossini@iastate.edu, phone: 515-294-8952

\*e-mail: lubach.joseph@gene.com

\*e-mail: nagapudi.karthik@gene.com

<sup>&</sup>lt;sup>1</sup>Iowa State University, Department of Chemistry, Ames, IA, USA, 50011.

<sup>&</sup>lt;sup>2</sup>Center of Interdisciplinary Magnetic Resonance, National High Magnetic Field Laboratory, 1800 East Paul Dirac Drive, Tallahassee, FL 32310, USA.

<sup>&</sup>lt;sup>3</sup>Genentech Inc., South San Francisco, CA, USA, 94080.

#### **ABSTRACT**

Active pharmaceutical ingredients (APIs) can be prepared in many different solid forms and phases that affect their physicochemical properties and suitability for oral dosage forms. The development and commercialization of dosage forms require analytical techniques that can determine and quantify the API phase in the final drug product. <sup>13</sup>C solid-state NMR (SSNMR) spectroscopy is widely employed to characterize pure and formulated solid APIs; however, <sup>13</sup>C SSNMR experiments on dosage forms with low API loading are often challenging due to low sensitivity and interference from excipients. Here, fast MAS <sup>1</sup>H SSNMR experiments are shown to be applicable for the rapid characterization of low drug load formulations. Diagnostic <sup>1</sup>H SSNMR spectra of APIs within tablets are obtained by using combinations of frequency-selective saturation and excitation pulses, 2D experiments and <sup>1</sup>H spin diffusion periods. Selective saturation pulses efficiently suppress the broad <sup>1</sup>H SSNMR signals from the most commonly encountered excipients such as lactose and cellulose, allowing observation of high frequency API <sup>1</sup>H NMR signals. <sup>1</sup>H SSNMR provides a one to three orders of magnitude reduction in experiment time compared to standard <sup>13</sup>C SSNMR experiments, enabling diagnostic SSNMR spectra of dilute APIs within tablets to be obtained within a few minutes. The <sup>1</sup>H SSNMR spectra can be used for quantification provided calibrations are performed on a standard sample with known API loading.

### **KEYWORDS**

Polymorph, Oral Dosage Forms, Phase Characterization, Active Pharmaceutical Ingredients, Molecular Structure

#### INTRODUCTION

Active pharmaceutical ingredients (APIs) exist in numerous distinct solid phases (e.g., polymorphs, cocrystals, salts, amorphous dispersions, etc.) and their physicochemical properties determine the performance of the API within solid dosage forms such as tablets. 1-3 13 C crosspolarization magic angle spinning (CPMAS) solid-state NMR (SSNMR) spectroscopy is widely applied for the identification, characterization, and quantification of pure and formulated solid APIs. 4-7 Different solid API phases usually give rise to distinct 13C solid-state NMR spectra with unique <sup>13</sup>C chemical shifts. <sup>4-7</sup> However, the intrinsically poor sensitivity of natural isotopic abundance <sup>13</sup>C SSNMR spectroscopy and the low concentration of APIs (typically 2 to 35 wt.%) often make it challenging to detect and characterize APIs in dosage forms by SSNMR. Prior <sup>13</sup>C SSNMR studies of formulated drug products have shown that <sup>13</sup>C SSNMR spectra diagnostic of the API phase can be acquired even for API loadings down to ca. 1 wt.% in favorable cases. 7-11 But, it is well known that APIs and organic solids can have long <sup>1</sup>H longitudinal relaxation times  $(T_1)$  on the order of hundreds of seconds. <sup>12–16</sup> APIs with long <sup>1</sup>H  $T_1$  will have substantially reduced sensitivity for <sup>13</sup>C SSNMR and it is challenging or impossible to study such APIs by <sup>13</sup>C SSNMR in formulations with low drug loads. Additionally, excipient materials in the formulation give rise to NMR signals that overlap/interfere with those from the API. Interference is especially problematic for <sup>1</sup>H and <sup>13</sup>C SSNMR experiments because most excipients are organic materials. 17,18 Alternatively, NMR signals from the API can be selectively detected by probing NMR-active elements such as fluorine, <sup>19,20</sup> nitrogen, <sup>17,21</sup> sodium, <sup>22</sup> and chlorine <sup>18,23</sup> that are exclusive to the API. Unfortunately, these NMR experiments are often infeasible because of poor sensitivity and/or absence of these elements in the API.

Dynamic nuclear polarization (DNP)<sup>24–26</sup> and fast magic angle spinning (MAS)<sup>27</sup> are often employed to enhance the sensitivity of SSNMR experiments by orders of magnitude. DNP has provided order of magnitude gains in SSNMR sensitivity, enabling  $^{13}$ C,  $^{15}$ N, and  $^{35}$ Cl SSNMR experiments on a range of pure and formulated APIs. $^{17,23,26,28,29}$  DNP is especially helpful for NMR experiments on APIs with long  $^{1}$ H  $T_{1}$ . $^{30,31}$  But, DNP currently requires specialized hardware, cryogenic sample temperatures and methods for doping the sample with stable radicals, which may cause unanticipated changes in the solid form of an API. $^{32}$  The achievable DNP sensitivity enhancements are also highly sample dependent. $^{17,23,26,28}$ 

Fast MAS increases the sensitivity of SSNMR by providing access to high resolution <sup>1</sup>H SSNMR spectra and/or enabling proton detection of heteronuclei. <sup>27,33,34</sup> Fast MAS and/or homonuclear decoupling (*i.e.*, CRAMPS) are routinely used to obtain high resolution <sup>1</sup>H SSNMR spectra of pure APIs. <sup>4,5,34–40</sup> Brown and co-workers applied CRAMPS double-quantum single-quantum (DQ-SQ) <sup>1</sup>H-<sup>1</sup>H 2D NMR experiments to differentiate hydrated and anhydrous forms of an API in a dosage form of unspecified API loading. <sup>41</sup> They also showed fast MAS DQ-SQ experiments can detect and resolve minor polymorphic forms within mixtures of pure APIs down to a loading of 1 wt.%. <sup>42</sup> Zhou and Rienstra have previously applied fast MAS and proton detection to obtain 2D <sup>1</sup>H-<sup>13</sup>C HETCOR spectra of an ibuprofen tablet with high API loading (*ca.* 65 wt.%). <sup>43</sup> Though, proton detected 2D <sup>1</sup>H { <sup>13</sup>C} SSNMR experiments are unlikely to provide significant gains in sensitivity as compared to direct detection 1D <sup>13</sup>C CPMAS SSNMR with large diameter rotors.

Here, we investigate the feasibility of using fast MAS  $^1$ H SSNMR experiments ( $v_{rot} \ge 50$  kHz) to rapidly detect and characterize dilute APIs in commercial and model dosage forms.  $^1$ H SSNMR offers much greater sensitivity than  $^{13}$ C SSNMR because of the 100% natural isotopic

abundance and high gyromagnetic ratio of <sup>1</sup>H. To the best of our knowledge, fast MAS <sup>1</sup>H SSNMR spectroscopy has not been demonstrated as a method to detect APIs in realistic dosage forms, likely because the limited resolution of <sup>1</sup>H SSNMR spectra causes intense <sup>1</sup>H NMR signals from the abundant excipients to overlap with and obscure the <sup>1</sup>H NMR signals from the dilute API. To address this problem, we describe how <sup>1</sup>H NMR signals from APIs in a formulation can be selectively detected by using pulse sequences that exploit combinations of selective excitation (SE) pulses, selective saturation pulses (SSPs) and spin diffusion (SD) periods. Comparison of fast MAS <sup>1</sup>H and traditional <sup>13</sup>C CPMAS SSNMR spectra shows that <sup>1</sup>H SSNMR typically provides an order of magnitude reduction in experiment time. <sup>1</sup>H solid-state NMR experiments on polymorphs and model formulations demonstrate that <sup>1</sup>H solid-state NMR experiments can be used to detect different solid drug forms. The enhanced NMR sensitivity provided by <sup>1</sup>H SSNMR is shown to be useful for experiments on formulations with low API loading and APIs that have long <sup>1</sup>H longitudinal relaxation times (*T*<sub>1</sub>).

### **Experimental**

Sample Preparation. Pure API samples, lactose monohydrate, magnesium stearate, and microcrystalline cellulose (MCC) were purchased from Sigma-Aldrich and used without further purification. Commercial tablets of mecl (All Day Less Drowsy Dramamine-brand, 25 mg API dose, manufactured by Medtech Products Inc.), phenaz (Azo-brand, 97.5 mg API dose, manufactured by i-Health Inc.), phenyl (Sudafed PE-brand, 10 mg API dose, manufactured by McNeil Consumer Healthcare) were purchased from CVS Pharmacy. The API wt.% in the commercial tablets was determined by dividing the reported API dose by the total measured mass of the tablet (Table S1). Polymorphs of mexi were prepared from the as received mexi-I

according to previously reported syntheses, <sup>18,44</sup> with some slight modifications. **mexi-II** was prepared by dissolving 100 mg of **mexi-I** in ca. 2 mL of methanol, then slowly recrystallizing mexi-II over a period of 5 days. Mexi-III was prepared by heating 100 mg of mexi-I at 160 °C in an oven for 2 hours. Model formulations were prepared for pheny (20.8 mg pheny, 276.8 mg MCC) and mexi (29.8 mg mexi-I, 5.81 mg mexi-III, 75.9 mg MCC) by thoroughly mixing the constituent powders in a vortex mixer for 5 minutes. Polymorphs of **theo** were prepared from the as received commercial sample of **theo-II** according to previously reported syntheses. <sup>32,45</sup> **theo-**M was synthesized by slowly recrystallizing 100 mg of theo-II in an excess of water. Normally, theo-I is obtained by holding theo-II at 270°C for 2 hours, 45 however, with this procedure theo-II was typically obtained. Instead, theo-I was obtained by holding theo-M at 270 °C for 2 hours. A model formulation of theo was prepared by thoroughly mixing 5 mg of theo-I, 9.8 mg of theo-II and 84.9 mg of MCC. 2 wt. %, 4 wt. % and 6.1 wt. % mixtures of theo-II in MCC were prepared by using the following masses for each component. 2 wt. % theo-II (2 mg theo-II in 97.8 mg MCC). 4 wt. % theo-II (4 mg theo-II in 96.2 mg MCC). 6.1 wt. % theo-II (6.1 mg theo-II in 93.8 mg MCC).

Solid-State NMR Spectroscopy. All samples were gently ground into a powder using a motor and pestle prior to packing into 1.3 mm or 4 mm zirconia rotors for solid-state NMR experiments.  $^{1}$ H and all  $^{13}$ C SSNMR experiments were performed on a 400 MHz ( $B_0 = 9.4$  T) Bruker Avance III HD spectrometer equipped with broadband double resonance HX 1.3 mm fast MAS and 4 mm HX probes. Additional  $^{1}$ H solid-state NMR (SSNMR) experiments were performed on a 800 MHz ( $B_0 = 18.8$  T) Bruker Avance III spectrometer at the National High Field Magnetic Laboratory (NHFML) in Tallahassee, Florida equipped with a Bruker triple resonance HCN 1.3 mm fast MAS probe.  $^{1}$ H SSNMR spectra were indirectly referenced to neat

tetramethylsilane ( $\delta_{iso} = 0$  ppm) using adamantane ( $\delta_{iso} = 1.82$  ppm) and the unified scale in the IUPAC standard. Chemical shifts were referenced to neat tetramethylsilane ( $\delta_{iso} = 0$  ppm) by setting the high frequency peak of adamantane to 38.48 ppm. All SSNMR spectra were processed using the TopSpin v3.5 software package.

 $^{1}$ H SSNMR experiments at both fields were performed with MAS frequencies of 50 kHz. See Figure S1 for the pulse sequences used in this work. Rotor-synchronized  $^{1}$ H spin echo (400 MHz) or DEPTH $^{47}$  (800 MHz) experiments were used to minimize background signals from the probes and rotor caps in 1D NMR spectra.  $^{1}$ H longitudinal relaxation time constants ( $T_{1}$ ) were measured with saturation recovery spin echo pulse sequences. The recycle delay for 1D NMR experiments was typically set to 1.3 or 5 times the  $^{1}$ H  $T_{1}$  measured for the pure API.

 $2D^{-1}H^{-1}H$  spin diffusion (SD) NMR spectra were collected with (or without) selective saturation pulses (SSPs) (Figure S1). 2D SD NMR spectra were typically obtained with 4 scans per increment,  $t_1$  was incremented in steps of 40  $\mu$ s (25 kHz indirect dimension spectral width). Typically 130 to 160 hyper-complex  $t_1$ -increments were acquired, corresponding to respective acquisition times of 2.6 to 3.2 ms in the indirect dimension. Total experiment times are indicated on the various Figures. SSPs were applied on resonance with common excipient molecules (at ca. 3.5 ppm) saturated nearly all of the excipient  $^{-1}H$  NMR signals with minimal effect on the high frequency NMR signals of the APIs (Figure S2). The SSP pulse length was 6 ms in all cases and the power and z-filter delay following the SSP ( $\tau_{ZF}$ ) was directly optimized on each sample to suppress the excipient  $^{-1}H$  NMR signals and minimize signal loss from high frequency API signals.  $\tau_{ZF}$  was between 20  $\mu$ s and 20 ms depending on the sample, with shorter  $\tau_{ZF}$  used when  $^{-1}H$  spin diffusion between high and low frequency API signals was fast. The SSP typically used RF fields of less than 1 kHz. The SSP was typically applied at an offset of 3 – 4.5 ppm, near to

the peak maximum of **MCC**. However, at lower field, the SSP offset needs to be carefully optimized because  $^{1}$ H spin diffusion is likely more rapid (see Figure S19 for an example of optimization of the SSP offset). For 9.4 T experiments on **mexi** an alternative SSP condition was used: three 6 ms saturation pulses were applied at a transmitter frequency of *ca.* 2.9 ppm and each SSP was separated by spin diffusion periods ( $\tau_{SSP}$ ) of 20 ms. The 1D and 2D SD NMR experiments typically used spin diffusion delays between 5 and 70 ms. 1D selective-excitation spin diffusion (SE-SD) experiments were conducted at  $B_0 = 18.8$  T with a 600  $\mu$ s low-power rectangular selective excitation pulse (*ca.* 400 Hz RF field) applied on resonance with high frequency API signals. The 1D SE-SD NMR spectra were obtained with the same pulse sequence as the 2D  $^{1}$ H $^{-1}$ H NOE experiments except without any evolution in  $t_1$  (Figure S1C). For experiments on **theo** at 9.4 T DANTE pulse trains  $^{48,49}$  were used for selective-excitation. The DANTE excitation pulses consisted of a train of fifteen 0.2  $\mu$ s pulses, each separated by two rotor cycles (40  $\mu$ s). The rf field of the 0.2  $\mu$ s pulses was 85 kHz.

All  $^{13}$ C MAS ( $v_{rot}$  = 8 kHz) SSNMR experiments were performed at 9.4 T with a triple resonance Bruker HXY probe configured in double resonance mode to maximize sensitivity. MAS  $^{13}$ C SSNMR spectra were obtained with cross-polarization to enhance sensitivity. $^{50}$   $^{13}$ C SSNMR spectra were acquired with the CP-TOSS sequence with a 243-step phase cycle. $^{51,52}$  The  $^{1}$ H CP spin lock pulse was linearly ramped between 90% and 100% of the spin lock RF field to broaden the Hartmann-Hahn match condition. $^{53}$  The length of the contact pulse was between 1.5 and 2.5 ms and was optimized on each sample. SPINAL-64 heteronuclear decoupling  $^{54}$  with an RF field of ca. 80 kHz was used for all  $^{13}$ C NMR experiments

Powder X-ray diffraction. Powder X-ray diffraction was used to confirm that the **mexi** polymorph synthesis was successful (Figure S3). Powder X-ray Diffraction (PXRD) patterns of

all of the samples were obtained using a Rigaku Ultima U4 XRD, with a CuK $\alpha$  source ( $\lambda$  = 1.540562 Å). A 2 $\theta$  range of 5° to 50° was scanned in stepwise fashion (step size = 0.05°, dwell = 2 seconds) for a total acquisition time of ca. 20 mins per sample.

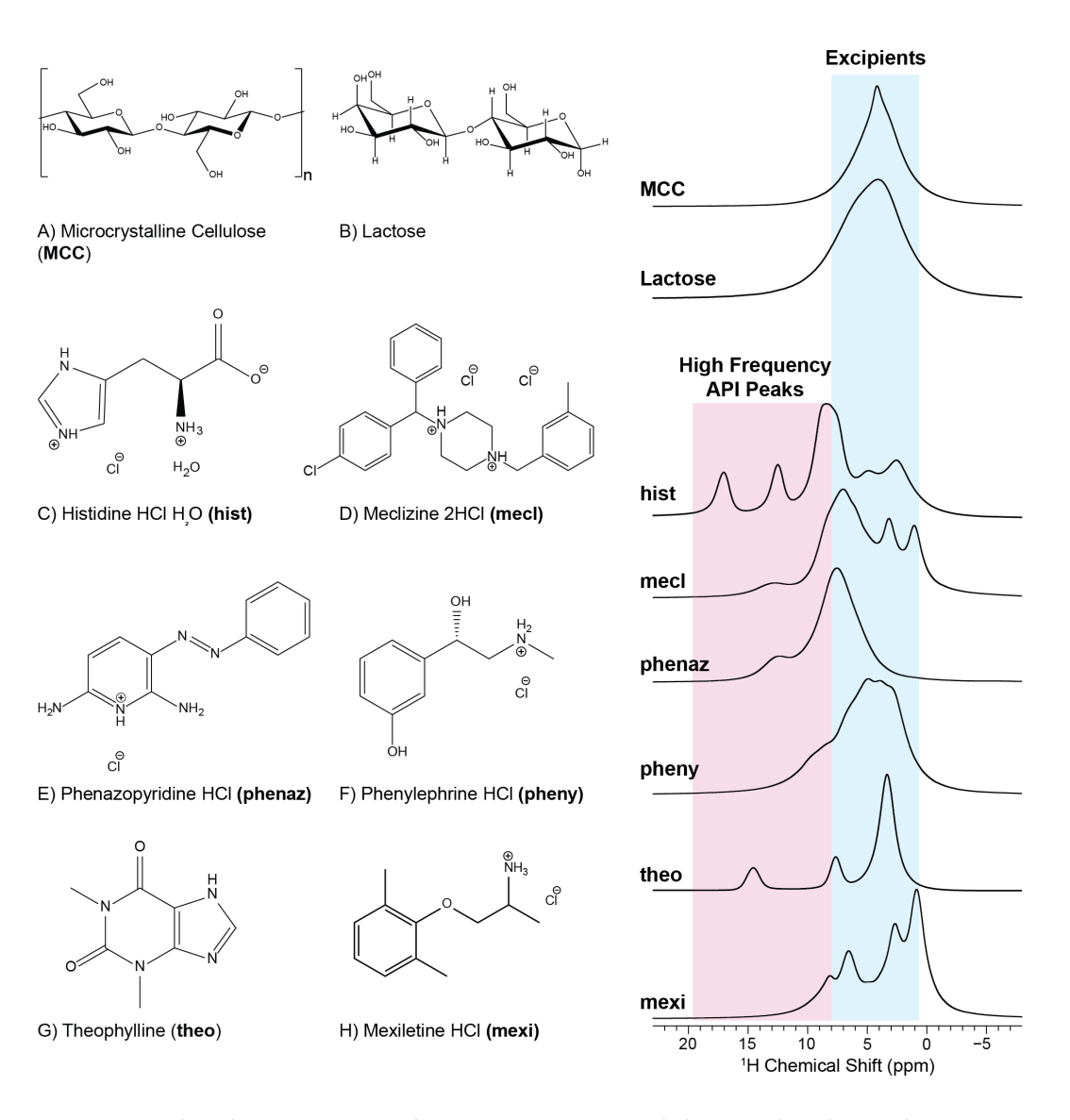


**Figure 1.** Molecular structures of (A-B) common excipient molecules and (C-H) representative small molecules/APIs used in this work. 1D  $^{1}$ H SSNMR spectra of each compound are shown in the right column. All  $^{1}$ H SSNMR spectra were obtained with a 50 kHz MAS frequency at  $B_0 = 9.4$  T.

#### RESULTS AND DISCUSSION

Fast MAS  $^{1}H$  SSNMR Spectra of Representative APIs and Typical Excipients. Figure 1 shows the molecular structures of representative APIs investigated in this study. Molecular structures are also shown for commonly encountered excipients such as microcrystalline cellulose (MCC) and lactose. These excipients are the major components of many tablets. Figure 1 and Figure S4 shows  $^{1}H$  SSNMR spectra of the APIs and excipients obtained with a MAS frequency ( $v_{rot}$ ) of 50 kHz and  $B_0 = 9.4$  T (400 MHz  $^{1}H$  Larmor frequency). Inspection of Figure 1 shows that MCC and lactose give rise to relatively broad and featureless  $^{1}H$  NMR spectra that span a frequency range of ca. 0 to 7 ppm. The  $^{1}H$  SSNMR spectra of MCC and lactose are relatively featureless because they possess numerous hydroxyl protons and alkyl protons with similar  $^{1}H$  chemical shifts. On the other hand, many of the APIs have well-resolved, high frequency  $^{1}H$  NMR signals that are separated from the excipient  $^{1}H$  NMR signals. These high frequency  $^{1}H$  NMR peaks typically arise from hydrogen atoms in amine, ammonium, and carboxylic acid functional groups.  $^{33,37,40-42}$  The high frequency  $^{1}H$  NMR signals can be used to observe the  $^{1}H$  SSNMR spectra of the APIs within formulations.

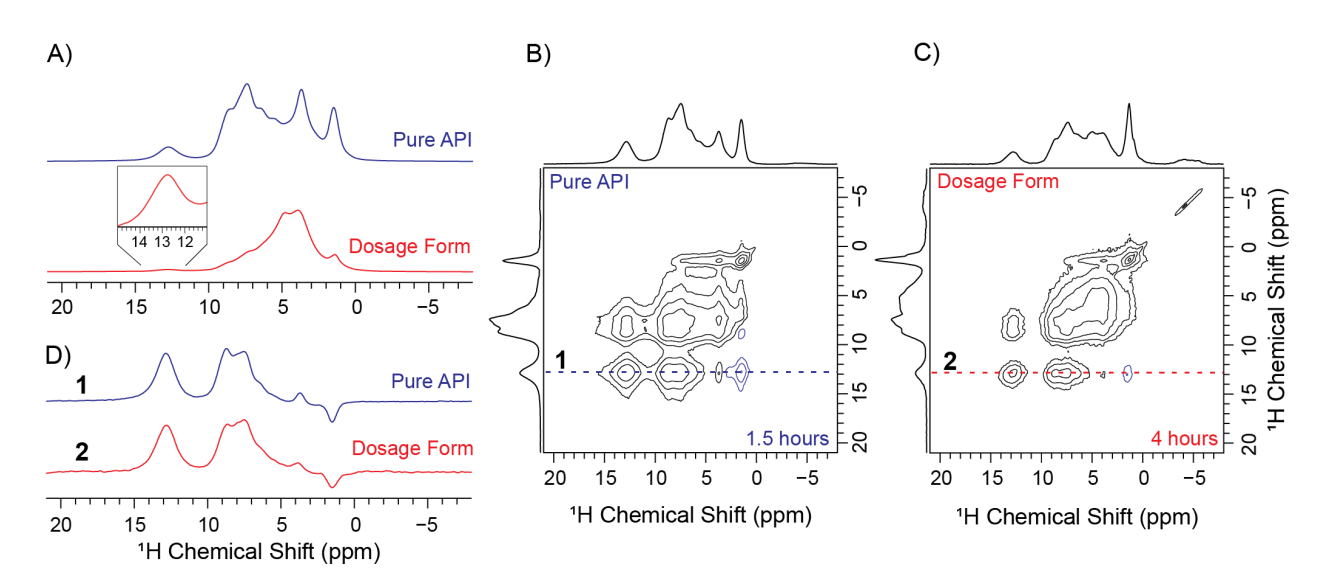


**Figure 2.** MAS <sup>1</sup>H SSNMR spectra of pure **mecl** and a commercial 12.5 wt.% **mecl** tablet acquired at  $B_0 = 18.8$  T with  $v_{rot} = 50$  kHz. A) 1D DEPTH NMR spectra. B), C) 2D <sup>1</sup>H SD NMR spectra acquired with a selective saturation pulse applied at 3.5 ppm and a 20 ms spin diffusion time. D) <sup>1</sup>H NMR spectra extracted from rows of the 2D NMR spectra (dashed lines in B and C).

Fast MAS  $^{1}H$  SSNMR Spectra of Commercial Dramamine® Tablets. 1D  $^{1}H$  SSNMR experiments on the antihistamine API meclizine dihydrochloride (**mecl,** Figure 1) and a commercial Dramamine® Less Drowsy tablet with 12.5 wt.% **mecl** loading illustrate the challenges of obtaining  $^{1}H$  SSNMR spectra of an API within a low drug load formulation (Figure 2A). The  $^{1}H$  SSNMR spectrum of the pure **mecl** obtained with a 50 kHz MAS frequency and  $B_0 = 18.8$  T shows several distinct isotropic  $^{1}H$  chemical shifts, including a high frequency signal at 12.7 ppm attributed to the ammonium group. The 18.8 T  $^{1}H$  SSNMR spectrum of the **mecl** tablet is dominated by the intense NMR signals from the excipient molecules, namely **MCC**. The intense **MCC** signals obscure most of the **mecl** signals; however, the  $^{1}H$  NMR signal of the ammonium group of **mecl** is resolved at 12.7 ppm (Figure 2A, inset). Protons with high chemical shifts are often involved in hydrogen bonding and are diagnostic of the solid form.  $^{33,37,40-42,55}$  The chemical

shift of the ammonium group is identical in the tablet and pure API, immediately suggesting the same API phase is present in both samples.

Additional <sup>1</sup>H NMR signals from the API may be required for phase identification, especially for APIs that can exist in multiple solid forms. Combinations of frequency-selective saturation and excitation pulses, 2D NMR spectra, and spin diffusion periods can be used to eliminate NMR signals from the excipients and obtain diagnostic <sup>1</sup>H SSNMR spectra of the API in formulations. Under fast MAS, homonuclear <sup>1</sup>H spin diffusion is slowed and resolved <sup>1</sup>H NMR signals can be suppressed with selective saturation pulses (SSPs) which typically consist of long duration pulses (1 to 30 ms) with a low RF field (less than 2 kHz). 56-58 The most commonly encountered excipient molecules have similar <sup>1</sup>H chemical shifts in the solid-state, centered around 3-5 ppm (Figure 1), consequently, SSPs applied in this region will eliminate or attenuate signals from most excipients. Note that the broad, overlapped <sup>1</sup>H SSNMR signals of **MCC** will lead to rapid <sup>1</sup>H spin diffusion amongst the <sup>1</sup>H spins in MCC, allowing the SSP to efficiently saturate the MCC <sup>1</sup>H NMR signal. High frequency acid or amine peaks from APIs are typically between 8 and 20 ppm<sup>33,37,40–42</sup> and are minimally affected by SSPs targeting the excipient resonances (Figure S2 and S4). Note that most APIs are marketed as free acids, salts, or cocrystals;<sup>59</sup> therefore, APIs will usually possess amine, ammonium, or acid functional groups that give rise to high frequency <sup>1</sup>H chemical shifts. 2D <sup>1</sup>H Spin Diffusion Experiments. 1D and 2D <sup>1</sup>H spin diffusion (SD) NMR experiments <sup>36,60</sup> enhance resolution and provide access to additional <sup>1</sup>H chemical shifts of the API (see Figure S1 for pulse sequences). 2D <sup>1</sup>H SD NMR experiments with SSPs were performed on pure **mecl** and the **mecl** tablet (Figures 2B and 2C). 2D <sup>1</sup>H SD NMR spectra of the **mecl** tablet could also be obtained without SSPs because the ammonium peak is well resolved (Figures S6 and S7). However, SSPs are required to reduce excipient signals in most tablets. <sup>1</sup>H spin diffusion occurs

during the delay  $(\tau_{SD})$  between the last two  $\pi/2$  pulses, producing additional API peaks in the rows of the 2D NMR spectra. Spin diffusion only occurs between <sup>1</sup>H nuclei that are proximate, <sup>61,62</sup> therefore, the NMR spectrum of the **mecl** tablet extracted from the ammonium peak row at 12.7 ppm will only show <sup>1</sup>H NMR signals from the API (dashed lines in Figure 2), assuming that the API is crystalline and phase segregated from the excipients. Figure 2D clearly shows that the same API phase is present in pure **mecl** and the **mecl** tablet, in agreement with <sup>13</sup>C SSNMR experiments (see below). The <sup>1</sup>H SSNMR spectra obtained from the rows of the 2D spin diffusion spectra are distinct from the <sup>1</sup>H spin echo NMR spectra because peak intensities depend upon the spin diffusion rates between the high frequency peak and the lower frequency peaks (cf. Figures 2A) and 2D). For isolated spins, spectral spin diffusion rates are determined by the strength of the dipolar coupling of the two coupled spins and the peak overlap integral evaluated at zero frequency. 63,64 The peak overlap integral is approximately inversely proportional to the square of the frequency difference. <sup>63,64</sup> For example, the ammonium peak shows rapid spin diffusion to the positively shifted aromatic <sup>1</sup>H NMR signals because the peaks have similar shifts and partially overlap at their baseline. On the other hand, the methyl and ammonium cross-peak has a low intensity and the cross-peak is negative. <sup>1</sup>H spin diffusion between the methyl protons and ammonium groups is likely slow because methyl and ammonium peaks are well separated ( $\Delta\delta \approx$ 11 ppm = 8.8 kHz at 18.8 T). Conventional ZO spin diffusion (<sup>1</sup>H-<sup>1</sup>H flip-flop) causes positive cross-peaks. We therefore speculate that the negative ammonium-methyl cross-peak could be caused by a double-quantum nuclear Overhauser effect (DQ-NOE) and this will be the subject of future study.

Notably, the 2D SD <sup>1</sup>H NMR spectra were obtained in a few hours and experiment times could be further accelerated by reducing the spin diffusion time to focus the observed direct dimension

signal into fewer API peaks or by acquiring fewer increments in the 2D experiment (with the tradeoff of reduced resolution in the indirect dimension). The data shown in Figure 2 were acquired at  $B_0 = 18.8$  T, but 2D  $^{1}$ H SD NMR experiments with SSPs were also successful at  $B_0 = 9.4$  T (Figure S8). The selectivity of the SSPs for excipient saturation is generally better at high field because  $^{1}$ H spin diffusion is slowed by increased  $^{1}$ H shift dispersion.

*1D Spin Diffusion Experiments*. If the chemical shift of a resolved API  $^1$ H NMR signal is known from prior characterization of pure API forms or from 1D  $^1$ H NMR experiments on the tablet, 1D selective excitation spin diffusion (SE-SD) NMR experiments can be performed (Figure S1C). In the 1D SE-SD NMR experiments on **mecl**, the ammonium peak at 12.7 ppm was selectively excited with a low-power 600 μs  $\pi/2$  pulse. The transverse  $^1$ H ammonium magnetization was then reconverted to longitudinal magnetization by a high-power broadband  $\pi/2$  pulse, which simultaneously saturates the other  $^1$ H NMR signals. The longitudinal  $^1$ H ammonium magnetization then undergoes spin diffusion for a fixed period of time, leading to the appearance of additional  $^1$ H chemical shifts, which can then be read by a final broadband  $\pi/2$  excitation pulse.

The 1D SE-SD method produces a high quality  $^{1}$ H SD NMR spectrum of the **mecl** tablet in only 30 minutes (Figure 3A). The 1D  $^{1}$ H SE-SD NMR spectrum of the **mecl** in the tablet obtained with a 70 ms spin diffusion time has a high signal-to-noise (SNR) ratio of ca. 44 for the characteristic ammonium peak, corresponding to a sensitivity (S) of 8.1 min $^{-1/2}$  ( $S = SNR \times t^{-1/2}$ , where t is the total experiment time in minutes). Different pulse shapes or excitation schemes $^{57,58,65}$  could likely improve the selectivity and efficiency of the SE pulses. For example, in later experiments on **theo**, simple DANTE schemes $^{48,49}$  were used for efficient frequency-selective excitation.

Comparison of <sup>1</sup>H and <sup>13</sup>C Solid-state NMR Spectroscopy. <sup>1</sup>H SSNMR experiments provide much better sensitivity than conventional <sup>13</sup>C CPMAS NMR experiments. A <sup>13</sup>C CPMAS spectrum

of the **mecl** tablet was obtained with a 4 mm rotor and had a SNR of 17 after 2 hours of signal averaging (Figure 3C and Figure S9). For the  $^{13}$ C SSNMR experiments  $S = 1.6 \text{ min}^{-1/2}$ , while the 1D  $^{1}$ H SSNMR spectrum of the **mecl** tablet had a S of 63 min $^{-1/2}$  and the 1D  $^{1}$ H SE-SD spectrum had a S of 8.1 min $^{-1/2}$  (Figure 3A and Figure S9). Comparing the sensitivity of the  $^{1}$ H and  $^{13}$ C SSNMR spectra shows that 1D  $^{1}$ H SSNMR offers 5– to 39–fold higher sensitivity for **mecl**, corresponding to 1 to 3 orders of magnitude reductions in experiment time as compared to  $^{13}$ C CPMAS. Note that the sensitivity of 1D SE-SD experiments could be further increased by reducing the  $^{1}$ H spin diffusion time to focus the NMR signal into fewer peaks, however, this would come at the expense of loss of intensity at other  $^{1}$ H chemical shifts.

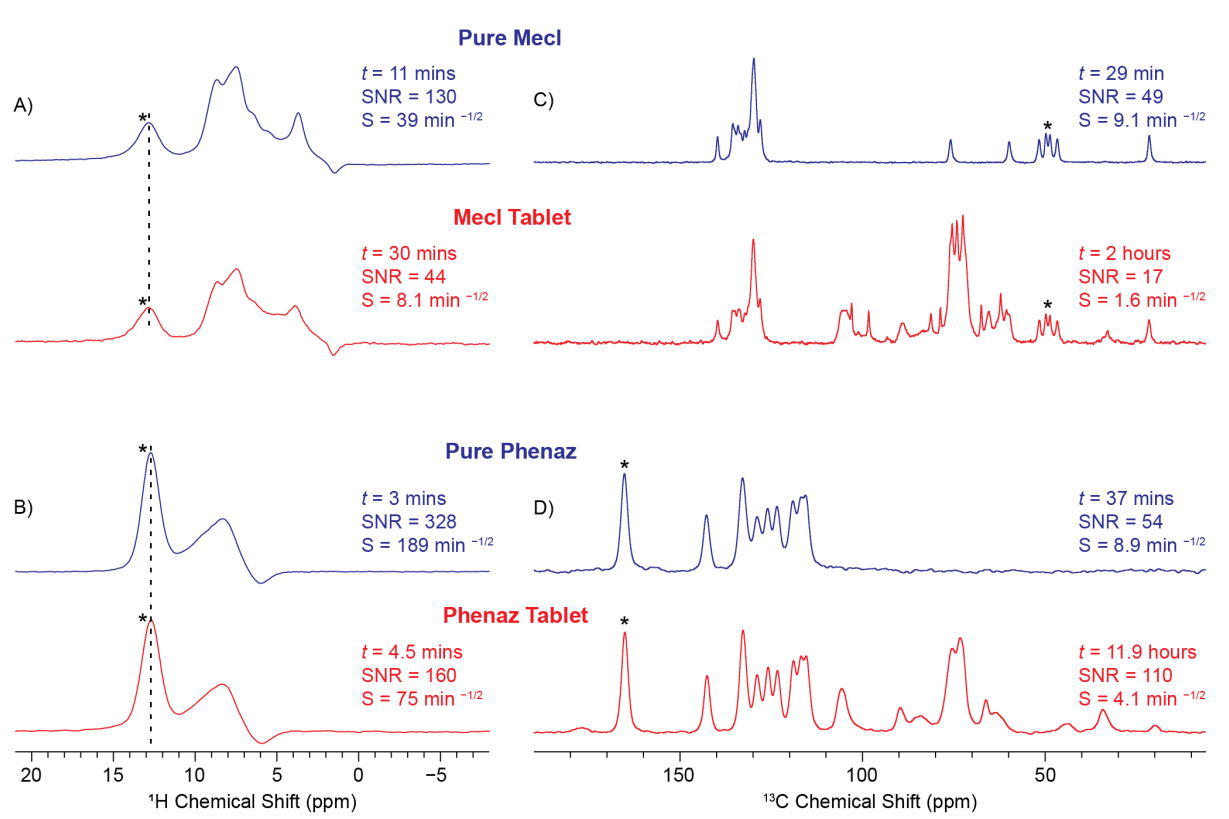


**Figure 3**. 1D <sup>1</sup>H SE-SD and <sup>13</sup>C CPMAS SSNMR spectra of A), C) pure **mecl** and a **mecl** tablet and B), D) pure **phenaz** and a **phenaz** tablet. The dashed line indicates the offset of the SE excitation pulse. Total experiment times are indicated. Spin diffusion times were 70 ms and 20 ms for **mecl** and **phenaz**, respectively. The <sup>1</sup>H SSNMR spectra were acquired at  $B_0 = 18.8$  T with  $v_{rot} = 50$  kHz and 1.3 mm rotors. <sup>13</sup>C CPMAS spectra were obtained at  $B_0 = 9.4$  T with  $v_{rot} = 8$  kHz and 4 mm rotors. Experiment time (*t*), signal-to-noise ratio (SNR) and sensitivity (*S*) are indicated for each spectrum. The asterisks denote the peaks used for determination of (SNR) and calculation of *S*.

Characterization of Other Commercial Formulations. Fast MAS <sup>1</sup>H SSNMR experiments were performed on other commercial API formulations to investigate the generality of our approach.

<sup>1</sup>H and <sup>13</sup>C SSNMR experiments on the API phenazopyridine hydrochloride (**phenaz**) and a commercial tablet with 68 wt.% API loading are summarized in Figures 3B and 3D (also Figures S10 and S11). Diagnostic <sup>1</sup>H SSNMR spectra of **phenaz** in the tablet were obtained in a few minutes with the 1D SE-SD pulse sequence (Figure 3B). The similarity of the 1D SE-SD spectra of the pure **phenaz** and the **phenaz** tablet suggests the same API phase is present in both. The 1D SE-SD spectrum of **phenaz** in the tablet showed a SNR of 160 after 4.5 minutes of signal averaging (S = 75 min<sup>-1/2</sup>), demonstrating the improved sensitivity provided by <sup>1</sup>H SSNMR spectroscopy. Comparing the 1D <sup>1</sup>H SE-SD spectrum and the <sup>13</sup>C CPMAS spectrum of the **phenaz** tablet shows that <sup>1</sup>H SSNMR provides an order of magnitude improvement in sensitivity, corresponding to a 100-fold reduction in experiment time. For example, consider a hypothetical 2 wt.% **phenaz** tablet: only 20 minutes would be required to obtain a 1D SE-SD <sup>1</sup>H SSNMR spectrum with a SNR of *ca*. 10, while *ca*. 4.5 days would be required to obtain a <sup>13</sup>C CPMAS with similar SNR.

The tablet Sudafed® PE containing 7 wt.% of the API phenylephrine hydrochloride (**pheny**) was also studied (Figure S12-S15). This tablet is challenging to characterize because it has a low API loading, pure **pheny** has a relatively long  ${}^{1}H$   $T_{1}$  of 18 s, and the API protons are present in a secondary ammonium group ( $C_{2}NH_{2}^{+}$ ) containing  ${}^{1}H$  spins that are strongly dipolar coupled, leading to broadening of the high frequency API  ${}^{1}H$  NMR signals. The secondary ammonium protons also have chemical shifts at ca. 10 ppm, close to the  ${}^{1}H$  chemical shift of many excipients. The overlapped  ${}^{1}H$  NMR signals make it challenging to selectively saturate the excipients, resulting in reduced intensity of the high frequency API signals. Despite these challenges, 2D  ${}^{1}H$  SSNMR spectra of the **pheny** tablet were obtained in 7 hours at  $B_{0} = 9.4$  T, while a  ${}^{13}C$  CPMAS

NMR spectrum of similar quality was obtained after 16 hours of signal averaging (Figures S15). Comparison of the <sup>13</sup>C CPMAS spectra of pure **pheny** and the tablet suggest that the API is likely amorphous in the tablet. This is reflected in the distinct appearance of the <sup>1</sup>H SSNMR spectra of the **pheny** tablet and pure **pheny**. In contrast, a model 7 wt.% **pheny** formulation made of a physical mixture of crystalline **pheny** and **MCC** yielded <sup>1</sup>H SSNMR spectra consistent with the crystalline phase (Figure S14). The experiments on **pheny** illustrate that <sup>1</sup>H SSNMR experiments are challenging when the <sup>1</sup>H NMR spectrum of the API suffers from overlap of many <sup>1</sup>H NMR signals and does not possess a well-resolved, high frequency <sup>1</sup>H NMR signal. In such cases <sup>13</sup>C CPMAS will likely be the preferred NMR method for interrogating the API phase within the tablet.

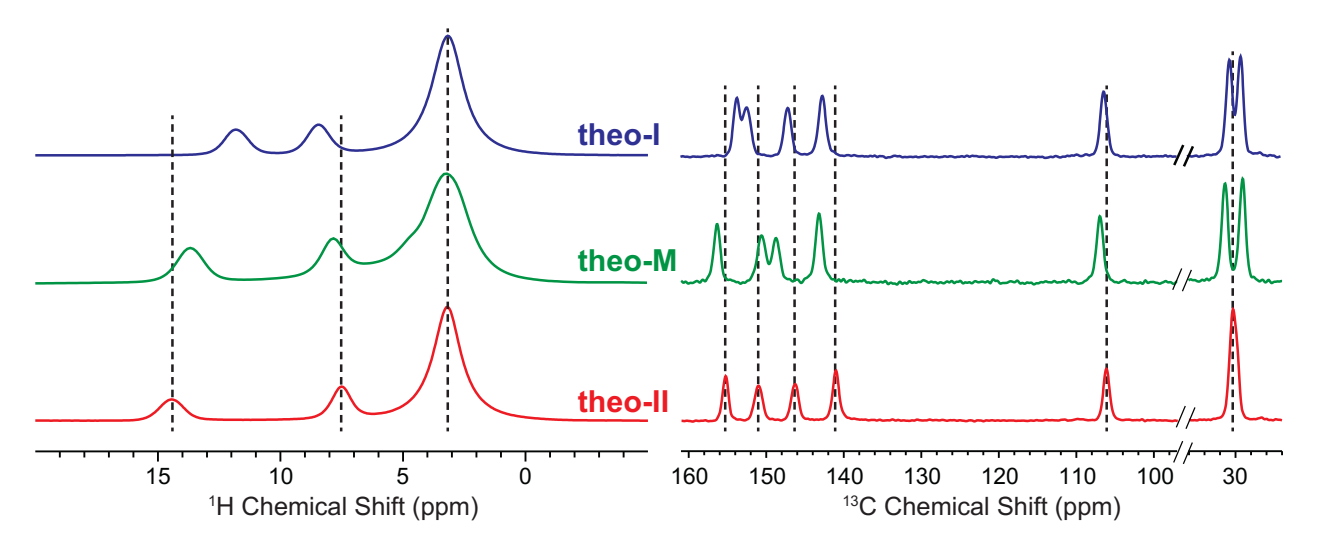


**Figure 4**. <sup>1</sup>H and <sup>13</sup>C CPMAS SSNMR spectra of theophylline form I (**theo-I**), theophylline monohydrate (**theo-m**), and theophylline form II (**theo-II**). <sup>1</sup>H SSNMR spectra were obtained with a 50 kHz MAS frequency at  $B_0 = 9.4$  T. <sup>13</sup>C SSNMR spectra were obtained with a 8 kHz MAS frequency at  $B_0 = 9.4$  T. Dashed lines are guides for the eye to illustrate the differences in isotropic chemical shifts.

Detection of Polymorphic Forms. It is well known that both <sup>1</sup>H chemical shifts<sup>37,39,40,55,66,67</sup> and SD rates<sup>33,35,66</sup> are very sensitive to differences in solid-state structure. Therefore, <sup>1</sup>H SSNMR should be an ideal technique to detect different API phases within formulations. To test this hypothesis, polymorphs of theophylline (**theo**) and mexiletine hydrochloride (**mexi**) and model

formulations were characterized by <sup>1</sup>H SSNMR. In addition to demonstrating the utility of our techniques to detect distinct solid phases in formulations, a critical aspect of pharmaceutical product development, these case studies provide examples of potential challenges for <sup>1</sup>H SSNMR (*i.e.*, slow <sup>1</sup>H longitudinal relaxation and poor separation of the high frequency API peaks from the excipients), and methods that can be used to overcome them.

Characterization of Theophylline Polymorphs. **Theo** has several stable crystal forms and a monohydrate form, all of which are readily accessible by simple recrystallization procedures. MAS <sup>1</sup>H and <sup>13</sup>C SSNMR spectra of theophylline form II (**theo-II**), theophylline form I (**theo-II**) and theophylline monohydrate (**theo-m**) are shown in Figure 4. The similarity of the <sup>1</sup>H and <sup>13</sup>C SSNMR spectra to those previously reported for the different polymorphs confirms the identity and purity of each polymorph. The 1D <sup>1</sup>H SSNMR spectra of the different **theo** forms illustrates that all forms are easily distinguished on the basis of the distinct <sup>1</sup>H chemical shifts observed for the amine (12-15 ppm) and methine (CH) protons (7.5-8.5 ppm). Baias *et al.* have noted that the differences in amine <sup>1</sup>H chemical shift occurs because of the distinct hydrogen bonding motifs encountered in the different crystal forms. The single crystal X-ray structure of **theo-II** shows the NH group forms a hydrogen bond to the nitrogen atom in the five-membered purine ring of an adjacent theophylline molecule. The NH group forms a hydrogen bond to a carbonyl group of an adjacent theophylline molecule in both **theo-m** and **theo-I.** 

 $^{1}$ H  $T_{1}$  measurements were performed on the different pure **theo** forms with both slow ( $v_{rot} = 8$  kHz) and fast MAS ( $v_{rot} = 50$  kHz) frequencies. Under slow MAS each  $^{1}$ H NMR signal showed a similar mono-exponential  $T_{1}$  because  $^{1}$ H spin diffusion is rapid between all  $^{1}$ H spins (Figure S16). The  $^{1}$ H  $T_{1}$  was ca. 53 s for **theo-I** and 64 s for **theo-II** (Table S2). Under fast MAS each  $^{1}$ H NMR signal had a distinct  $T_{1}$ ; for both **theo** forms the  $T_{1}$  of the methyl  $^{1}$ H was on the order of 60 s, while

the  $T_1$  of the high frequency amine  ${}^1\text{H}$  was much longer and between 300-460 s for the different forms (Table S3). The long  ${}^1\text{H}$   $T_1$  for the amine  ${}^1\text{H}$  of **theo** arises with fast MAS because  ${}^1\text{H}$  spin diffusion has been slowed and there are likely no dynamic motions of the amine groups at the correct frequencies to cause longitudinal relaxation. Fast MAS could reduce the sensitivity of SD  ${}^1\text{H}$  SSNMR experiments on **theo** where the amine signal will be excited because the amine  ${}^1\text{H}$   $T_1$  of several hundred seconds will dictate the recycle delay. Note that for the other compounds examined there were only slight differences in  $T_1$  measured for the different  ${}^1\text{H}$  NMR signals.

Previously, Taulelle and Nishiyama showed that RFDR recoupling can be applied to accelerate  $^{1}$ H spin diffusion under fast MAS and reduce the differences in  $^{1}$ H  $T_{1}$  between resolved  $^{1}$ H NMR signals. Alternatively, spin-lock pulses have been used to accelerate  $^{13}$ C spin diffusion when there is a large isotropic chemical shift difference. Here a low power H spin-lock pulse ( $v_{1}(^{1}\text{H}) \approx 15 \text{ kHz}$ ) with a duration of a 1.8 ms was used to enable H spin diffusion across the entire **theo** H NMR spectrum and transfer magnetization from the methyl H to the amine and methine H. The spin-lock pulse shortens the effective  $T_{1}$  of high frequency **theo** amine H NMR signals from several hundred seconds to less than 90 seconds (Table S3). Therefore, a H broadband  $\pi/2$  excitation pulse, spin-lock pulse, flip-back  $\pi/2$  pulse block was inserted prior to any SE pulses in the subsequent H SSNMR experiments on **theo** (Figure S1). For 1D SE-SD experiments on **theo** a spin-lock pulse was used to promote H spin diffusion in lieu of the usual longitudinal magnetization storage period (Figure S1E). Spin-lock pulses used to accelerate H spin diffusion in **theo** were between 600 μs and 1.8 ms in duration.

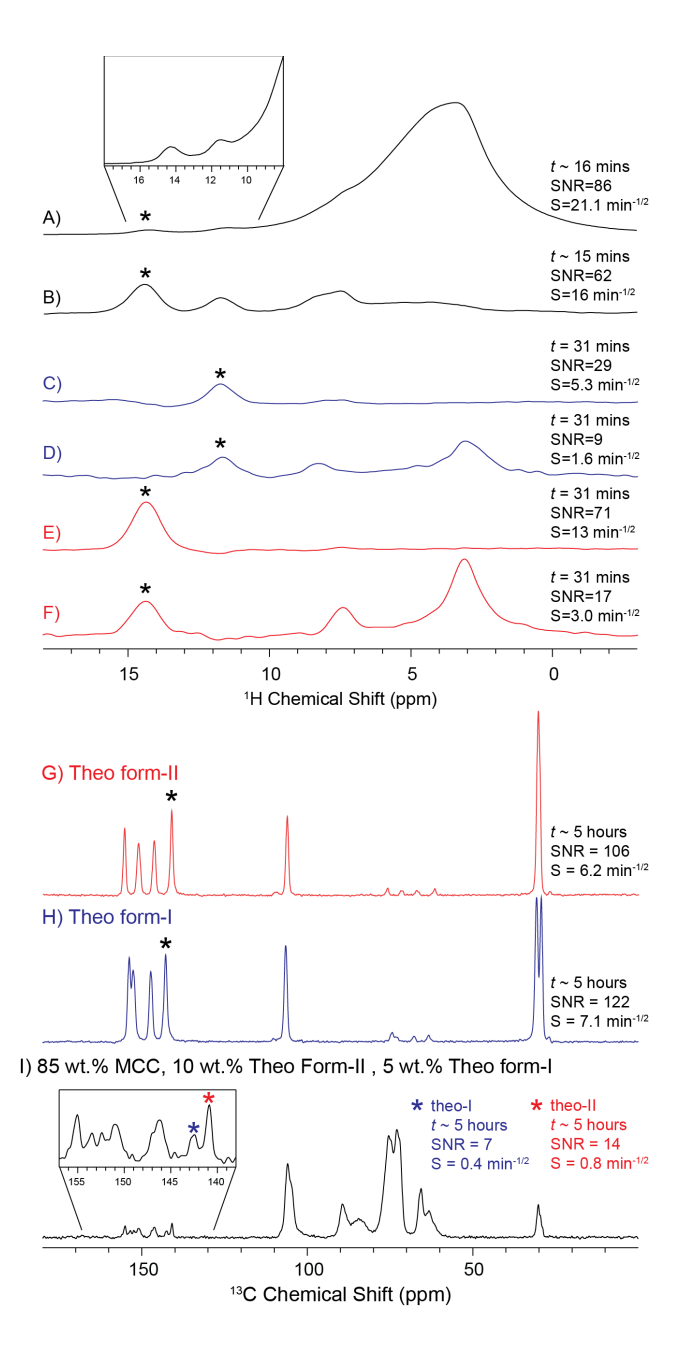


**Figure 5**. <sup>1</sup>H and <sup>13</sup>C SSNMR spectra of a physical mixture of 85 wt.% **MCC**, 10 wt.% **theo-II** and 5 wt.% **theo-I**. <sup>1</sup>H spin echo spectra recorded A) without and B) with SSP on resonance with **MCC**. (C-F) 1D SE-SD <sup>1</sup>H SSNMR spectra with the SE pulse on resonance with the high frequency amine <sup>1</sup>H NMR signal of (C, D) **theo-I** or (E, F) **theo-II**. <sup>1</sup>H SSNMR spectra in D) and F) were obtained with a 1.8 ms spin-lock pulse following the SE pulse to promote <sup>1</sup>H spin diffusion. Spectra in C) and E) were recorded with a 20 μs spin-lock pulse to minimize <sup>1</sup>H spin diffusion. <sup>1</sup>H SSNMR spectra were obtained with a 50 kHz MAS frequency at  $B_0 = 9.4$  T. <sup>13</sup>C SSNMR spectra were obtained with an 8 kHz MAS frequency at  $B_0 = 9.4$  T. Experiment times (t), signal-to-noise ratios (SNR) and sensitivity (S) are indicated. The asterisks denote the peaks used for determination of (SNR) and calculation of S.

NMR experiments were performed on mixtures of **theo** solid forms and **MCC** to demonstrate the potential of fast MAS <sup>1</sup>H SSNMR to rapidly detect different solid API forms when they are dilute within a formulation. A mixture consisting of 85 wt.% **MCC**, 10 wt.% **theo-II** and 5 wt.% **theo-I** was used in these initial experiments. This mixture mimics a scenario where there is a total drug load of 15 wt.% in the formulation and one-third of the API (**theo-II**) has undergone a transition to a secondary API phase (**theo-I**). In the 1D <sup>1</sup>H SSNMR spectrum obtained without SSPs, the high frequency amine signals of both **theo-I** and **theo-II** are obscured (Figure 5A, inset). Acquisition of a 1D <sup>1</sup>H SSNMR spectrum with SSPs helps suppress the **MCC** signals and clearly shows both amine and methine <sup>1</sup>H NMR signals for both **theo** forms (Figure 5B).

1D SE-SD NMR experiments were also performed with DANTE SE pulses on resonance with the amine signal of **theo-I** or **theo-II** (Figures 5C-5F). The 1D SE-SD <sup>1</sup>H SSNMR spectra obtained with a minimal spin diffusion time only show the respective amine chemical shifts (Figures 5C and 5E), while those recorded with a 1.8 ms spin-lock pulse to promote <sup>1</sup>H spin diffusion show additional chemical shifts from the methine and methyl groups (Figures 5D and 5F). The <sup>1</sup>H chemical shifts observed in the 1D SE-SD NMR spectra exactly match those observed in the <sup>1</sup>H NMR spectra of the corresponding pure phases (Figure 4), confirming the identity of the **theo** phases in the mixture.

Comparing the sensitivity of  $^{13}$ C and  $^{1}$ H SSNMR experiments on the **theo-MCC** mixture shows that  $^{1}$ H SSNMR once again provides far superior sensitivity. After 5 hours of signal averaging the  $^{13}$ C CPMAS spectrum of the mixture shows SNR of about 14 and 7 for characteristic  $^{13}$ C peaks of **theo-II** and **theo-I**, respectively. These SNR values correspond to a sensitivity of 0.8 min $^{-1/2}$  and 0.4 min $^{-1/2}$  for **theo-II** and **theo-I**, respectively. Note that the low sensitivity of  $^{13}$ C CPMAS for **theo** primarily arises because of its relatively long  $^{1}$ H  $T_{1}$  which requires a long recycle

delay over 1 minute to be used for optimal sensitivity. Despite the long  ${}^{1}H$   $T_{1}$ ,  ${}^{1}H$  SSNMR spectra of both **theo** forms within the mixture can be obtained in 15 – 30 minutes with a SNR of over 30. The sensitivity of the  ${}^{1}H$  SSNMR spectra recorded without any spin diffusion is 13 min $^{-1/2}$  and 5 min $^{-1/2}$  for **theo-II** and **theo-I**, respectively. The sensitivity provided by  ${}^{1}H$  SSNMR is about 16 times better than  ${}^{13}C$  CPMAS, corresponding to a *two order of magnitude reduction in experiment time*. This is why high quality  ${}^{1}H$  NMR spectra are obtained in only 15-30 minutes each, while the  ${}^{13}C$  CPMAS spectrum required hours of signal averaging.

The SSNMR experiments on the **theo-MCC** mixture illustrate why it is challenging to characterize formulations with low API loading by conventional  $^{13}$ C CPMAS. For example, consider a scenario where the **theo-II** loading is only around 2 wt.%, then approximately  $2.5 \, days$  of signal averaging would be required to obtain a  $^{13}$ C SSNMR spectrum with a SNR of 10. On the other hand, in only  $30 \, minutes$  a  $^{1}$ H SSNMR spectrum of a 2 wt.% mixture of **theo-II** in **MCC** with a SNR of about 18 was obtained (Figure S17). This example demonstrates the advantages of fast MAS  $^{1}$ H SSNMR for probing formulations with very low API loading and/or when the API possesses a long  $^{1}$ H  $T_{1}$ .

*Detection of Mexiletine Polymorphs*. Three polymorphic forms of mexiletine hydrochloride (**mexi**), referred to as **mexi-I**, **mexi-II**, and **mexi-III**, were also prepared and characterized by  ${}^{1}$ H SSNMR. These polymorphs have previously been characterized with X-ray diffraction as well as  ${}^{13}$ C and  ${}^{35}$ Cl SSNMR. ${}^{18,44}$  The distinct 1D  ${}^{1}$ H SSNMR spectra of the **mexi** polymorphs at  $B_0 = 9.4$  T suggests that  ${}^{1}$ H NMR should be useful to distinguish and quantify the different forms (Figure 6 and Figure S18). A model **mexi** formulation was prepared by mixing 5.2 wt.% **mexi-II**, 26.7 wt.% **mexi-I**, and 68.0 wt.% **MCC** (total API load of 32 wt.%). The model

**mexi** formulation mimics the composition of a tablet with 16% of the API converted to a secondary phase (**mexi-III**).

The **mexi** formulation is challenging to study by  ${}^{1}H$  SSNMR because the primary ammonium protons of **mexi** have chemical shifts of ca. 8 ppm, near to the  ${}^{1}H$  shifts of **MCC**. Therefore, SSP conditions that can completely saturate **MCC** signals and minimally perturb the **mexi** signals are required. Optimization of the SSP offset for **mexi-I**, **mexi-III** and **MCC** at  $B_0 = 9.4$  T showed that with a single SSP, the **MCC** signals can only be saturated when the SSP is applied at offsets of ca. 4.7 to 3.7 ppm, which falls within the **MCC** lineshape (Figure S19A). However, at these offsets the  ${}^{1}H$  NMR signals from **mexi-I** and **mexi-III** are also partially saturated, likely because the **mexi**  ${}^{1}H$  SSNMR spectra are poorly resolved at 9.4 T and  ${}^{1}H$  spin diffusion rapidly equilibrates polarization across the spectrum.

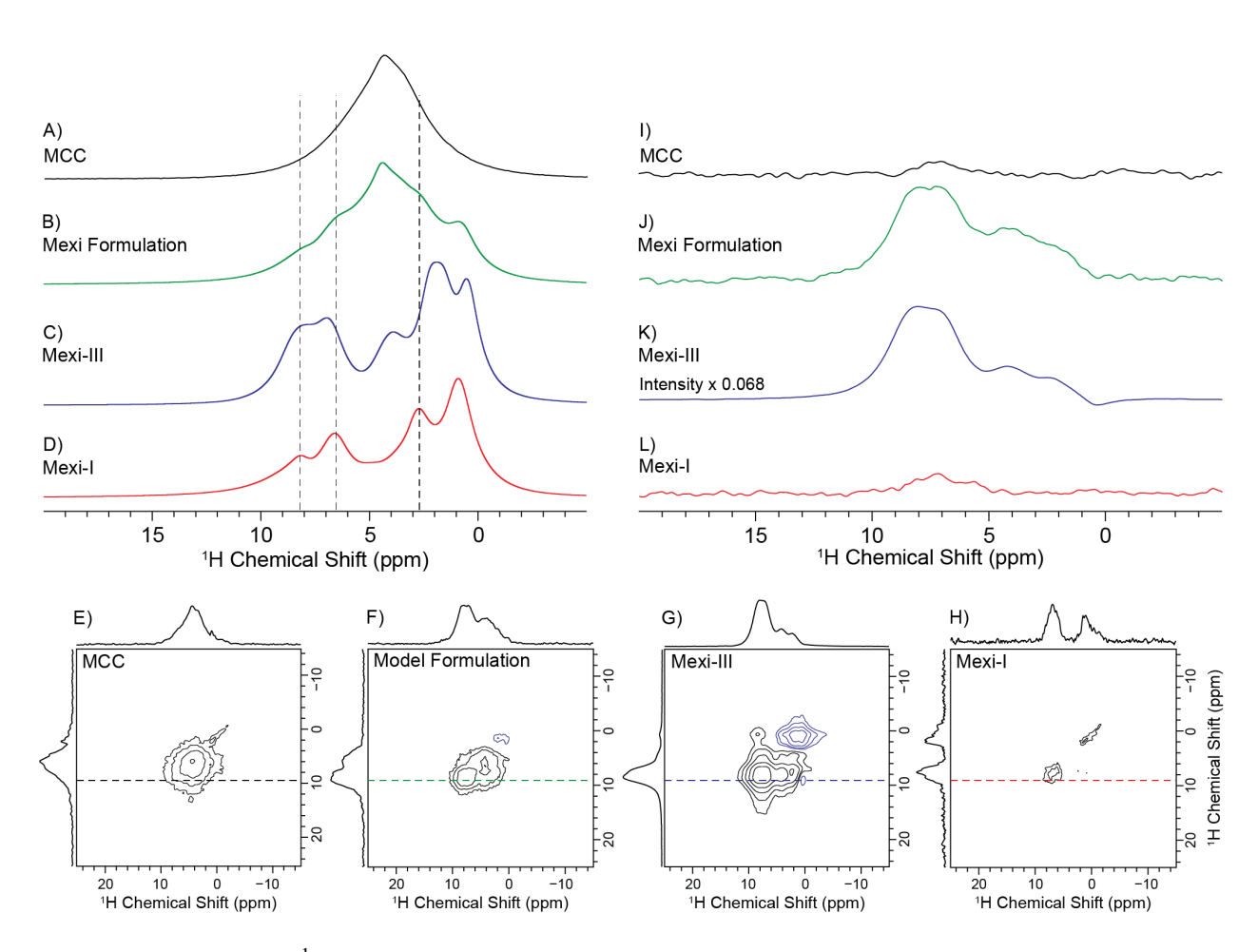


**Figure 6.** (A-D) 1D <sup>1</sup>H spin echo SSNMR spectra of **MCC**, the model **mexi** formulation, **mexi-III** and **mexi-I**. The **mexi** formulation consists of a physical mixture of 5.2 wt.% **mexi-III**, 26.7 wt.% **mexi-I**, and 68.0 wt.% **MCC**. Vertical dashed lines are guides for the eye to illustrate differences in <sup>1</sup>H chemical shifts for the two **mexi** polymorphs. (E-H) 2D <sup>1</sup>H SD NMR spectra of of **MCC**, the model **mexi** formulation, **mexi-III** and **mexi-I**. All spectra were recorded with a 20 ms spin diffusion mixing time and three SSPs applied at an offset of 2.8 ppm. (I-L) <sup>1</sup>H SSNMR spectra extracted from the indicated rows of the 2D <sup>1</sup>H SD NMR spectra. Only <sup>1</sup>H NMR signals from **mexi-III** are visible from the formulation.

Alternatively, application of three SSPs, each separated by a 20 ms z-filter/spin diffusion period, enables MCC signals to be saturated completely with SSP offsets of 2.0 to 5.0 (Figure S19B). 2D  $^{1}$ H SD NMR spectra acquired with SSP offsets below 3.0 ppm saturates the **mexi-I** and MCC signals, while **mexi-III** signals are still observable. 2D SD  $^{1}$ H NMR spectra with three SSPs applied at 2.9 ppm were acquired at  $B_0 = 9.4$  T from **mexi-I**, **mexi-III**, MCC and the model **mexi** 

formulation (Figure 6E-H). The rows extracted from the 2D SD <sup>1</sup>H NMR spectra at an indirect dimension shift of 9.7 ppm are shown in Figure 6I-L. As expected, only NMR signals from **mexi-III** are visible in the formulation because the SSPs efficiently saturate both **MCC** and **mexi-I** NMR signals. These results illustrate that <sup>1</sup>H SSNMR could be useful to selectively detect different polymorphic forms on the basis of their response to SSPs. However, a clear drawback of the <sup>1</sup>H SSNMR experiments that **mexi-I** NMR signals could not be observed in this case because they are attenuated by the SSPs required to eliminate **MCC** NMR signals. This limitation could likely be overcome by increasing the static magnetic field and/or MAS frequency to increase <sup>1</sup>H resolution, reduce spin diffusion and improve the selectivity of SSPs.

Quantification of API Loading by <sup>1</sup>H SSNMR. Finally, the ability of <sup>1</sup>H SSNMR to quantify API loading in a formulation was also tested. It has previously been demonstrated that <sup>13</sup>C CPMAS can be used to quantify API loading within a formulation based upon the comparison of peak intensities. <sup>7–11</sup> H SSNMR experiments were performed on physical mixtures of **theo-II** and **MCC** with variable loading of **theo-II** from 2 wt.% to 9.8 wt.% to investigate the possibility of using <sup>1</sup>H SSNMR for quantification of APIs in formulations. Figure 7A shows a plot of the integrated intensity of the amine <sup>1</sup>H NMR signal of **theo-II** measured with 1D SE-SD experiments as a function of the **theo-II** wt.%. For the calibration experiments the recycle delay was fixed to 95 s which corresponds to 1.3 times the signal build-up time constant of 73 s measured for the **theo-II** amine signal. The SE pulse was placed on resonance with the **theo-II** amine signal and the spin diffusion spin-lock pulse was set to 20 μs in duration to maximize sensitivity by focusing signal into the amine peak. Figure 7A shows that there is a linear correlation between the **theo-II** <sup>1</sup>H NMR signal intensity and the **theo-II** wt.% within the mixtures. Using the measured integrated intensities and the calibration equation, the average absolute error in the API loading was 0.36

wt.% and the average relative error was 9.9% of the expected API loading (Table S4). These experiments demonstrate fast MAS <sup>1</sup>H SSNMR should be quantitative, provided the <sup>1</sup>H NMR signal response to the SSP and SE pulses are first calibrated on standards with known API loading.

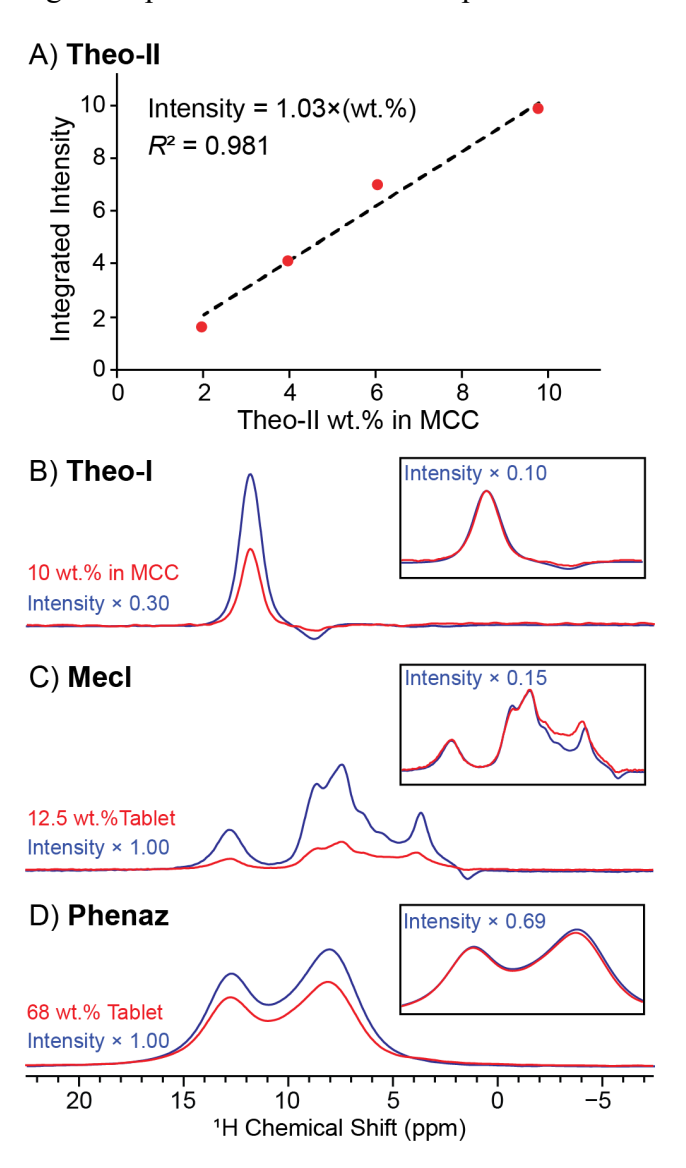


**Figure 7.** A) Plot of integrated intensity of the amine  ${}^{1}H$  NMR signal of **theo-II** on different mixtures with **MCC**. Comparison of the 1D SE-SD  ${}^{1}H$  NMR signal intensities for the corresponding pure APIs and for B) 10 wt.% **theo-I** in MCC, C) a 12.5 wt.% **mecl** tablet, D) a 68 wt.% **phenaz** tablet. The insets show the intensity scaling required to match the integrated intensity of high frequency API signals of the formulation to those of the pure API. The spectra are normalized for differences in number of scans. Data for A), B) and D) was obtained at  $B_0 = 9.4$  T and C) was obtained at  $B_0 = 18.8$  T.

Signal intensities were also used to estimate the loading of other APIs within formulations. 1D SE-SD <sup>1</sup>H NMR integrated signal intensities were compared for samples of pure **theo-I** and a 10 wt.% theo I – MCC physical mixture (Figure 7B). Based upon the integrated signal intensity the theo-I wt.% in the mixture was determined to be 11 wt.%, which is within 1 wt.% of the expected value. Comparison of the **mexi-III** signal intensity in 2D <sup>1</sup>H SD experiments yields a 6.8 wt.% loading of mexi-III in the formulation, which is close to the expected value of 5.2 wt.% mexi-III (Figure 6K). Quantification was also attempted with 1D SE-SD <sup>1</sup>H SSNMR experiments on pure and formulated mecl and phenaz (Figure 7). For the commercial mecl tablet an API loading of 15.0 wt.% was determined, which is within 2.5 wt.% of the stated mecl loading of 12.5 wt.%. Note that different  ${}^{1}H$   $T_{1}$  values were measured for **mecl** in bulk and dosage forms (Table S5). All NMR spectra of **mecl** were obtained with recycle delays of  $1.3 \times T_1$  for optimal sensitivity. However, there is likely some uncertainty in the measured  $T_1$  values and this will affect the accuracy of quantification. Quantification could be improved by using longer recycle delays to minimize the contributions of longitudinal relaxation to signal differences. For the commercial phenaz tablet the API loading was measured to be 69 wt. % which is within 1 wt.% of the expected value of 68 wt.%. The phenaz quantification was performed with 1D SE-SD experiments that used recycle delays of  $5 \times T_1$ . We anticipate that the accuracy of API quantification by <sup>1</sup>H SSNMR could be further improved by using common practices such as adding an internal standard to the sample, weighing the amount of sample packed into the rotor and/or limiting the sample to the central portion of the rotor to minimize rf homogeneity effects.

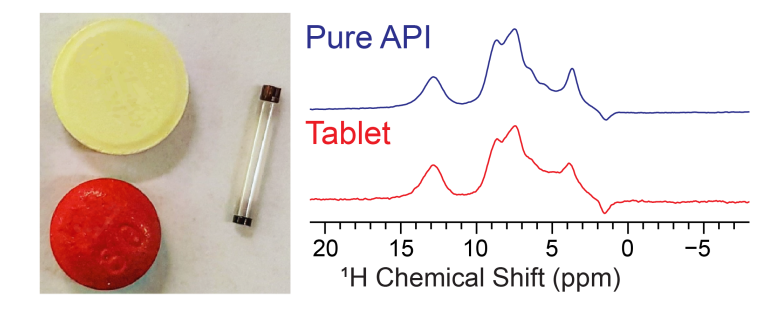
#### **CONCLUSIONS**

In summary, straightforward and highly sensitive 1D and 2D fast MAS  $^1$ H SSNMR experiments can be used to rapidly identify the solid forms of dilute APIs within dosage forms. The sensitivity of  $^1$ H SSNMR greatly exceeds that of  $^{13}$ C SSNMR, typically enabling one to three order of magnitude reductions in experiment times. Diagnostic  $^1$ H SSNMR spectra of dilute APIs within formulations can typically be obtained in minutes, even when the API has unfavorable  $T_1$  relaxation times and low API loading, whereas  $^{13}$ C SSNMR spectra would require hours or days of signal averaging to obtain NMR spectra of similar SNR.  $^1$ H SSNMR can permit the routine detection of many APIs that have a long  $^1$ H  $T_1$  and/or APIs that are very dilute in a formulation. For **theo** and **mexi** the  $^1$ H SSNMR spectra of different crystalline forms are distinct, allowing polymorphic forms to be identified and detected on the basis of  $^1$ H chemical shifts or on the basis of differential response to saturation and excitation pulses. Experiments on **theo** mixtures and other samples demonstrate that  $^1$ H SSNMR spectra are quantitative after calibration on the individual components of the formulation.

While many pharmaceutical samples are amenable to characterization using <sup>1</sup>H SSNMR experiments, such methods may not be applicable or useful for all APIs, as was observed for **pheny** and **mexi-I**. In cases where the API lacks high frequency <sup>1</sup>H NMR signals and/or has a poorly resolved <sup>1</sup>H NMR spectrum, both SSPs and SE pulses will be inefficient and it will be challenging to detect API <sup>1</sup>H NMR signals from the formulation and/or obtain meaningful structural information about the API. However, these limitations have some obvious solutions. The resolution of <sup>1</sup>H SSNMR spectra and SD rates can be reduced by using higher magnetic fields and/or faster MAS frequencies. Probes capable of MAS frequencies greater than 100 kHz are becoming widespread and should allow APIs with high frequency <sup>1</sup>H chemical shifts below 10

ppm to be studied.<sup>27,34</sup> Alternatively, DQ NMR experiments can provide improved resolution and shift discrimination,<sup>41,42</sup> at the expense of reduced sensitivity. While the focus of the current work has been on pharmaceuticals, the methods described here should also be applicable to study other complex mixtures of organic solids.

# **TOC Graphic**



#### SUPPORTING INFORMATION

Additional NMR spectra, experimental details and Bruker pulse programs. The Supporting Information is available free of charge on the ACS Publications website.

#### ACKNOWLEDGMENT

This material is based upon work supported by the National Science Foundation under Grant No. 1709972 to AJR. We thank Genentech, Inc. and its Innovation Fund, for providing additional financial support for this work. AJR also thanks Iowa State University for additional support. A portion of this work was performed at the National High Magnetic Field Laboratory, which is supported by the National Science Foundation Cooperative Agreement No. DMR-1644779 and the State of Florida.

#### REFERENCES

- (1) Hörter, D.; Dressman, J. B. Influence of physicochemical properties on dissolution of drugs in the gastrointestinal tract. *Adv. Drug Deliv. Rev.* **1997**, *25*, 3–14.
- (2) Huang, L.-F.; Tong, W.-Q. Impact of solid state properties on developability assessment of drug candidates. *Adv. Drug Deliv. Rev.* **2004**, *56*, 321–334.
- (3) Hilfiker, R. *Polymorphism*; Hilfiker, R., Ed.; Wiley-VCH: Weinheim, FRG, 2006.
- (4) Berendt, R. T.; Sperger, D. M.; Munson, E. J.; Isbester, P. K. Solid-state NMR spectroscopy in pharmaceutical research and analysis. *TrAC Trends Anal. Chem.* **2006**, *25*, 977–984.
- (5) Monti, G. A.; Chattah, A. K.; Linck, Y. G. In *Annual Reports on NMR Spectroscopy*; Elsevier Ltd., 2014; Vol. 83, pp 221–269.
- (6) Skorupska, E.; Jeziorna, A.; Kazmierski, S.; Potrzebowski, M. J. Recent progress in solid-state NMR studies of drugs confined within drug delivery systems. *Solid State Nucl. Magn. Reson.* **2014**, *57–58*, 2–16.
- (7) Harris, R. K.; Hodgkinson, P.; Larsson, T.; Muruganantham, A. Quantification of bambuterol hydrochloride in a formulated product using solid-state NMR. *J. Pharm. Biomed. Anal.* **2005**, *38*, 858–864.
- (8) Sanchez, S.; Ziarelli, F.; Viel, S.; Delaurent, C.; Caldarelli, S. Improved solid-state NMR quantifications of active principles in pharmaceutical formulations. *J. Pharm. Biomed. Anal.* **2008**, *47*, 683–687.
- (9) Virtanen, T.; Maunu, S. L. Quantitation of a polymorphic mixture of an active pharmaceutical ingredient with solid state 13C CPMAS NMR spectroscopy. *Int. J. Pharm.* **2010**, *394*, 18–25.
- (10) Zielińska-Pisklak, M.; Pisklak, D. M.; Wawer, I. Application of 13C CPMAS NMR for Qualitative and Quantitative Characterization of Carvedilol and its Commercial Formulations. *J. Pharm. Sci.* **2012**, *101*, 1763–1772.

- (11) Tinmanee, R.; Larsen, S. C.; Morris, K. R.; Kirsch, L. E. Quantification of gabapentin polymorphs in gabapentin/excipient mixtures using solid state 13 C NMR spectroscopy and X-ray powder diffraction. *J. Pharm. Biomed. Anal.* **2017**, *146*, 29–36.
- (12) Ganapathy, S.; Naito, A.; McDowell, C. A. Paramagnetic doping as an aid in obtaining high-resolution carbon-13 NMR spectra of biomolecules in the solid state. *J. Am. Chem. Soc.* **1981**, *103*, 6011–6015.
- (13) Brown, C. E. Effects of chemical modification and cobalt(II) chloride addition on the carbon-13 NMR spectra of carnosine as a solid powder. *J. Am. Chem. Soc.* **1982**, *104*, 5608–5610.
- (14) Alemany, L. B.; Grant, D. M.; Pugmire, R. J.; Alger, T. D.; Zilm, K. W. Cross polarization and magic angle sample spinning NMR spectra of model organic compounds. 1. Highly protonated molecules. *J. Am. Chem. Soc.* **1983**, *105*, 2133–2141.
- (15) Nelson, B. N.; Schieber, L. J.; Barich, D. H.; Lubach, J. W.; Offerdahl, T. J.; Lewis, D. H.; Heinrich, J. P.; Munson, E. J. Multiple-sample probe for solid-state NMR studies of pharmaceuticals. *Solid State Nucl. Magn. Reson.* **2006**, *29*, 204–213.
- (16) Lou, X.; Shen, M.; Li, C.; Chen, Q.; Hu, B. Reduction of the 13C cross-polarization experimental time for pharmaceutical samples with long T1 by ball milling in solid-state NMR. *Solid State Nucl. Magn. Reson.* **2018**, *94*, 20–25.
- (17) Rossini, A. J.; Widdifield, C. M.; Zagdoun, A.; Lelli, M.; Schwarzwälder, M.; Copéret, C.; Lesage, A.; Emsley, L. Dynamic Nuclear Polarization Enhanced NMR Spectroscopy for Pharmaceutical Formulations. *J. Am. Chem. Soc.* **2014**, *136*, 2324–2334.
- (18) Namespetra, A. M.; Hirsh, D. A.; Hildebrand, M. P.; Sandre, A. R.; Hamaed, H.; Rawson, J. M.; Schurko, R. W. 35 Cl solid-state NMR spectroscopy of HCl pharmaceuticals and their polymorphs in bulk and dosage forms. *CrystEngComm* **2016**, *18*, 6213–6232.
- (19) Wenslow, R. M. 19 F Solid-State NMR Spectroscopic Investigation of Crystalline and Amorphous Forms of a Selective Muscarinic M 3 Receptor Antagonist, in Both Bulk and Pharmaceutical Dosage Form Samples. *Drug Dev. Ind. Pharm.* **2002**, *28*, 555–561.
- (20) Brus, J.; Urbanova, M.; Sedenkova, I.; Brusova, H. New perspectives of 19F MAS NMR in the characterization of amorphous forms of atorvastatin in dosage formulations. *Int. J. Pharm.* **2011**, *409*, 62–74.
- (21) Patel, J. R.; Carlton, R. A.; Yuniatine, F.; Needham, T. E.; Wu, L.; Vogt, F. G. Preparation and Structural Characterization of Amorphous Spray-Dried Dispersions of Tenoxicam with Enhanced Dissolution. *J. Pharm. Sci.* **2012**, *101*, 641–663.
- (22) Burgess, K. M. N.; Perras, F. A.; Lebrun, A.; Messner-Henning, E.; Korobkov, I.; Bryce, D. L. Sodium-23 Solid-State Nuclear Magnetic Resonance of Commercial Sodium Naproxen and its Solvates. *J. Pharm. Sci.* **2012**, *101*, 2930–2940.
- (23) Hirsh, D. A.; Rossini, A. J.; Emsley, L.; Schurko, R. W. 35 Cl dynamic nuclear polarization solid-state NMR of active pharmaceutical ingredients. *Phys. Chem. Chem. Phys.* **2016**, *18*,

25893-25904.

- (24) Maly, T.; Debelouchina, G. T.; Bajaj, V. S.; Hu, K.-N.; Joo, C.-G.; Mak–Jurkauskas, M. L.; Sirigiri, J. R.; van der Wel, P. C. a; Herzfeld, J.; Temkin, R. J.; Griffin, R. G. Dynamic nuclear polarization at high magnetic fields. *J. Chem. Phys.* **2008**, *128*, 052211.
- (25) Ni, Q. Z.; Daviso, E.; Can, T. V; Markhasin, E.; Jawla, S. K.; Swager, T. M.; Temkin, R. J.; Herzfeld, J.; Griffin, R. G. High Frequency Dynamic Nuclear Polarization. *Acc. Chem. Res.* **2013**, *46*, 1933–1941.
- (26) Zhao, L.; Pinon, A. C.; Emsley, L.; Rossini, A. J. DNP-enhanced solid-state NMR spectroscopy of active pharmaceutical ingredients. *Magn. Reson. Chem.* **2018**, 1–27.
- (27) Deschamps, M. Ultrafast Magic Angle Spinning Nuclear Magnetic Resonance. *Annu. Reports NMR Spectrosc.* **2014**, *81*, 109–144.
- (28) Ni, Q. Z.; Yang, F.; Can, T. V.; Sergeyev, I. V.; D'Addio, S. M.; Jawla, S. K.; Li, Y.; Lipert, M. P.; Xu, W.; Williamson, R. T.; Leone, A.; Griffin, R. G.; Su, Y. In Situ Characterization of Pharmaceutical Formulations by Dynamic Nuclear Polarization Enhanced MAS NMR. *J. Phys. Chem. B* **2017**, *121*, 8132–8141.
- (29) Zhao, L.; Hanrahan, M. P.; Chakravarty, P.; DiPasquale, A. G.; Sirois, L. E.; Nagapudi, K.; Lubach, J. W.; Rossini, A. J. Characterization of Pharmaceutical Cocrystals and Salts by Dynamic Nuclear Polarization-Enhanced Solid-State NMR Spectroscopy. *Cryst. Growth Des.* 2018, 18, 2588–2601.
- (30) Rossini, A. J.; Zagdoun, A.; Hegner, F.; Schwarzwälder, M.; Gajan, D.; Copéret, C.; Lesage, A.; Emsley, L. Dynamic nuclear polarization NMR spectroscopy of microcrystalline solids. *J. Am. Chem. Soc.* **2012**, *134*, 16899–16908.
- (31) Pinon, A. C.; Schlagnitweit, J.; Berruyer, P.; Rossini, A. J.; Lelli, M.; Socie, E.; Tang, M.; Pham, T.; Lesage, A.; Schantz, S.; Emsley, L. Measuring Nano- to Microstructures from Relayed Dynamic Nuclear Polarization NMR. *J. Phys. Chem. C* **2017**, *121*, 15993–16005.
- (32) Pinon, A. C.; Rossini, A. J.; Widdifield, C. M.; Gajan, D.; Emsley, L. Polymorphs of Theophylline Characterized by DNP Enhanced Solid-State NMR. *Mol. Pharm.* **2015**, *12*, 4146–4153.
- (33) Brown, S. P. Applications of high-resolution 1H solid-state NMR. *Solid State Nucl. Magn. Reson.* **2012**, *41*, 1–27.
- (34) Nishiyama, Y. Fast magic-angle sample spinning solid-state NMR at 60–100kHz for Natural Abundance Samples. *Solid State Nucl. Magn. Reson.* **2016**.
- (35) Elena, B.; Pintacuda, G.; Mifsud, N.; Emsley, L. Molecular Structure Determination in Powders by NMR Crystallography from Proton Spin Diffusion. *J. Am. Chem. Soc.* **2006**, *128*, 9555–9560.
- (36) Brown, S. P. Probing proton–proton proximities in the solid state. *Prog. Nucl. Magn. Reson. Spectrosc.* **2007**, *50*, 199–251.

- (37) Salager, E.; Stein, R. S.; Pickard, C. J.; Elena, B.; Emsley, L. Powder NMR crystallography of thymol. *Phys. Chem. Chem. Phys.* **2009**, *11*, 2610.
- (38) Vogt, F. G.; Clawson, J. S.; Strohmeier, M.; Edwards, A. J.; Pham, T. N.; Watson, S. A. Solid-State NMR Analysis of Organic Cocrystals and Complexes. *Cryst. Growth Des.* **2009**, *9*, 921–937.
- (39) Baias, M.; Widdifield, C. M.; Dumez, J.-N.; Thompson, H. P. G.; Cooper, T. G.; Salager, E.; Bassil, S.; Stein, R. S.; Lesage, A.; Day, G. M.; Emsley, L. Powder crystallography of pharmaceutical materials by combined crystal structure prediction and solid-state 1H NMR spectroscopy. *Phys. Chem. Chem. Phys.* **2013**, *15*, 8069.
- (40) Widdifield, C. M.; Robson, H.; Hodgkinson, P. Furosemide's one little hydrogen atom: NMR crystallography structure verification of powdered molecular organics. *Chem. Commun.* **2016**, *52*, 6685–6688.
- (41) Griffin, J. M.; Martin, D. R.; Brown, S. P. Distinguishing Anhydrous and Hydrous Forms of an Active Pharmaceutical Ingredient in a Tablet Formulation Using Solid-State NMR Spectroscopy. *Angew. Chemie Int. Ed.* **2007**, *46*, 8036–8038.
- (42) Maruyoshi, K.; Iuga, D.; Watts, A. E.; Hughes, C. E.; Harris, K. D. M.; Brown, S. P. Assessing the Detection Limit of a Minority Solid-State Form of a Pharmaceutical by 1 H Double-Quantum Magic-Angle Spinning Nuclear Magnetic Resonance Spectroscopy. *J. Pharm. Sci.* **2017**, *106*, 3372–3377.
- (43) Zhou, D. H.; Rienstra, C. M. Rapid Analysis of Organic Compounds by Proton-Detected Heteronuclear Correlation NMR Spectroscopy with 40 kHz Magic-Angle Spinning. *Angew. Chemie Int. Ed.* **2008**, *47*, 7328–7331.
- (44) Hildebrand, M.; Hamaed, H.; Namespetra, A. M.; Donohue, J. M.; Fu, R.; Hung, I.; Gan, Z.; Schurko, R. W. 35 Cl solid-state NMR of HCl salts of active pharmaceutical ingredients: structural prediction, spectral fingerprinting and polymorph recognition. *CrystEngComm* 2014, 16, 7334.
- (45) Fucke, K.; McIntyre, G. J.; Wilkinson, C.; Henry, M.; Howard, J. A. K.; Steed, J. W. New Insights into an Old Molecule: Interaction Energies of Theophylline Crystal Forms. *Cryst. Growth Des.* **2012**, *12*, 1395–1401.
- (46) Harris, R. K.; Becker, E. D.; Cabral de Menezes, S. M.; Granger, P.; Hoffman, R. E.; Zilm, K. W. Further conventions for NMR shielding and chemical shifts (IUPAC Recommendations 2008). Pure Appl. Chem. 2008, 80, 59–84.
- (47) Cory, D. .; Ritchey, W. . Suppression of signals from the probe in bloch decay spectra. *J. Magn. Reson.* **1988**, *80*, 128–132.
- (48) Bodenhausen, G.; Freeman, R.; Morris, G. A. A Simple Pulse Sequence for Selective Excitation in Fourier-Transform Nmr. *J. Magn. Reson.* **1976**, *23*, 171–175.
- (49) Morris, G. A.; Freeman, R. Selective excitation in Fourier transform nuclear magnetic resonance. *J. Magn. Reson.* **1978**, *29*, 433–462.

- (50) Pines, A.; Gibby, M. G.; Waugh, J. S. Proton- Enhanced Nuclear Induction Spectroscopy. A Method for High Resolution NMR of Dilute Spins in Solids. *J. Chem. Phys.* **1972**, *56*, 1776–1777.
- (51) Song, Z.; Antzutkin, O. N.; Feng, X.; Levitt, M. H. Sideband suppression in magic-angle-spinning NMR by a sequence of 5 π pulses. *Solid State Nucl. Magn. Reson.* **1993**, *2*, 143–146.
- (52) Antzutkin, O. N. Sideband manipulation in magic-angle-spinning nuclear magnetic resonance. *Prog. Nucl. Magn. Reson. Spectrosc.* **1999**, *35*, 203–266.
- (53) Peersen, O. B.; Wu, X. L.; Kustanovich, I.; Smith, S. O. Variable-Amplitude Cross-Polarization MAS NMR. *J. Magn. Reson. Ser. A* **1993**, *104*, 334–339.
- (54) Fung, B. M.; Khitrin, A. K.; Ermolaev, K. An Improved Broadband Decoupling Sequence for Liquid Crystals and Solids. *J. Magn. Reson.* **2000**, *142*, 97–101.
- (55) Santos, S. M.; Rocha, J.; Mafra, L. NMR Crystallography: Toward Chemical Shift-Driven Crystal Structure Determination of the β-Lactam Antibiotic Amoxicillin Trihydrate. *Cryst. Growth Des.* **2013**, *13*, 2390–2395.
- (56) Robertson, A. J.; Pandey, M. K.; Marsh, A.; Nishiyama, Y.; Brown, S. P. The use of a selective saturation pulse to suppress t 1 noise in two-dimensional 1 H fast magic angle spinning solid-state NMR spectroscopy. *J. Magn. Reson.* **2015**, *260*, 89–97.
- (57) Brinkmann, A.; Kentgens, A. P. M. Proton-Selective 17 O– 1 H Distance Measurements in Fast Magic-Angle-Spinning Solid-State NMR Spectroscopy for the Determination of Hydrogen Bond Lengths. *J. Am. Chem. Soc.* **2006**, *128*, 14758–14759.
- (58) Mithu, V. S.; Tan, K. O.; Madhu, P. K. Selective inversion of 1H resonances in solid-state nuclear magnetic resonance: Use of double-DANTE pulse sequence. *J. Magn. Reson.* **2013**, 237, 11–16.
- (59) Paulekuhn, G. S.; Dressman, J. B.; Saal, C. Trends in Active Pharmaceutical Ingredient Salt Selection based on Analysis of the Orange Book Database. *J. Med. Chem.* **2007**, *50*, 6665–6672.
- (60) Caravatti, P.; Neuenschwander, P.; Ernst, R. R. Characterization of Heterogeneous Polymer Blends by Two-Dimensional Proton Spin Diffusion Spectroscopy. *Macromolecules* **1985**, *18*, 119–122.
- (61) Schmidt-Rohr, K.; Spiess, H. W. *Multidimensional Solid-State NMR and Polymers*; Academic Press Ltd.: London, UK, 1994.
- (62) Peter Cheung, T. T. In *Encyclopedia of Magnetic Resonance*; John Wiley & Sons, Ltd: Chichester, UK, 2007; Vol. 84, pp 83–121.
- (63) Suter, D.; Ernst, R. R. Spectral spin diffusion in the presence of an extraneous dipolar reservoir. *Phys. Rev. B* **1982**, *25*, 6038–6041.

- (64) Ernst, M.; Meier, B. H. In *Solid State NMR of Polymers*; Ando, I., Asakura, T., Eds.; Elsevier B.V., 1998; pp 83–121.
- (65) Freeman, R. Selective excitation in high-resolution NMR. *Chem. Rev.* **1991**, *91*, 1397–1412.
- (66) Elena, B.; Emsley, L. Powder Crystallography by Proton Solid-State NMR Spectroscopy. *J. Am. Chem. Soc.* **2005**, *127*, 9140–9146.
- (67) Oikawa, T.; Okumura, M.; Kimura, T.; Nishiyama, Y. Solid-state NMR meets electron diffraction: determination of crystalline polymorphs of small organic microcrystalline samples. *Acta Crystallogr. Sect. C Struct. Chem.* **2017**, *73*, 219–228.
- (68) Ye, Y. Q.; Malon, M.; Martineau, C.; Taulelle, F.; Nishiyama, Y. Rapid measurement of multidimensional 1H solid-state NMR spectra at ultra-fast MAS frequencies. *J. Magn. Reson.* **2014**, *239*, 75–80.
- (69) Robyr, P.; Meier, B. H.; Ernst, R. R. Radio-frequency-driven nuclear spin diffusion in solids. *Chem. Phys. Lett.* **1989**, *162*, 417–423.